Aerosol Science and Technology, 40:664–671, 2006

ISSN: 0278-6826 print / 1521-7388 online
DOI: 10.1080/02786820600793951

Submicron Salt Particle Production in Bubble Bursting

Lynn M. Russell[1] and Elizabeth G. Singh[2]
[1]*Scripps Institution of Oceanography, University of California, San Diego, La Jolla, California, USA*
[2]*Dupont Chemical Solutions Enterprise, Deepwater, New Jersey, USA*

Laboratory experiments of bubble bursting have shown that particle production increases with concentration for aqueous solutions of NaCl (Spiel 1998). Here, experiments with a submicron Na particle counter for three Na salts—NaCl, NaBr, and NaI—show comparable trends. Similarities in behavior are evident when the concentration for each salt is normalized to a threshold concentration (Lessard and Zieminski 1971). The number, size, and mass of particles produced increase with normalized solution concentration, suggesting that the same transition that controls ionic entropy and self-diffusion in aqueous solutions will govern the bubble bursting process. Further insight into the controlling forces is provided by the prediction of the number, size, and mass of particles produced from the Eotvos number, the ratio of buoyant to surface forces of the aqueous solution. The similarities among the parameterizations of particle properties to the Eotvos number for all three Na salts provide a strong indication that, for similar density solutions, particle production is dominated by surface forces, independent of chemical compositions. A complete mechanistic interpretation of particle production is limited by our inability to capture (theoretically or experimentally) both the macroscopic fluid mechanics of film rupture and the microscopic intermolecular interactions of strong ionic solutions. However, the parameterizations to dimensionless quantities of aqueous solutions presented here are sufficient to predict the essential characteristics of particle production. The collapse of the experimental results to common curves for several different salts shows the predictive ability of these parameterizations for other mixtures.

INTRODUCTION

A key source of marine aerosol results from the breaking of waves in the ocean, a process that produces particles ranging from tens of nanometers to hundreds of micrometers in diameter (Blanchard and Woodcock 1957; Smith et al. 1993; O'Dowd et al. 1997; Clarke et al. 2003). The complexity of this process on several scales has meant that quantitative predictions of this important particle source has relied on empirical correlations of particle production to ambient wind and wave conditions and to laboratory-controlled bubbling characteristics. Many studies were directed at the large aerosol mass associated with supermicron sea salt particles and lacked the instrumentation required to measure particles smaller than 100 nm diameter. This work characterizes the range of particle sizes from 20 to 300 nm, since salt particles in this size range play an important role in the indirect effect of marine particles on cloud radiative properties (Russell et al. 1994).

Few studies have investigated the role of chemical composition and concentration of the bubbled solution, which has become increasingly prominent because of recent studies of the variability of the sea surface microlayer and its role in forming salt particles (Guichard and Lamauve 1988; Cloke et al. 1991; Aluwihare et al. 1997; Martensson et al. 2003). The surfactant properties of organic compounds that constitute the microlayer could change the properties of sea salt particles produced. Scenarios for global change also include predictions of shifts in the concentrations of salts in the ocean. Incorporating these spatial and temporal variations in composition into global climate models requires a process-based understanding of particle formation from bubble bursting.

The challenge in understanding this type of particle formation begins with the variability of the atmospheric environment, preventing controlled observations in situ. To avoid this ambient variability, laboratory simulations of ocean waves in tanks are used to isolate individual breaking waves. Further simplification to individual bubble bursting in simulated saltwater uses clean air streams to carry particles for accurate monitoring. At this benchtop scale, particles can be accurately counted and associated with bubble bursting. The few available studies have produced snapshots of particle formation characteristics. More comprehensive studies are needed to provide the functional link between particle formation and solution characteristics. This study shows the link of particle formation to Na salt solution composition, which may be used as a general framework for a wider range of experiments on a variety of chemical compositions—including mixtures of salts and trace organic constituents—in the future.

Received 21 May 2004; accepted 17 October 2005.
The authors are grateful for financial support from the Office of Naval Research (N00014-97-1-0673; N00014-98-0565) and the National Science Foundation (ATM-0408501). Helpful comments from Sandra Troian and Donald Koch are also appreciated.
Address correspondence to Lynn M. Russell, Scripps Institute of Oceanography, 9500 Gilman Dr. Mail Code 0221, University of Calfornia, San Diego, La Jolla, CA 92093, USA. E-mail: lmrussell@uscd.edu

APPROACH

The breaking of a wave typically captures air that rises in millimeter-sized bubbles back to the surface. A capillary tube is used to produce bubbles of constant, predictable size (Blanchard and Syzdek 1988; Spiel 1997). The diameter of the bubble is given by equating the buoyant and surface forces at the tip of the capillary as the bubble is forming (Blanchard and Syzdek 1977)

$$d_b^3(\rho_l - \rho_a)g = 6d_c\sigma_l \quad [1]$$

where d_b is bubble diameter, $d_c = 2$ mm is capillary inner diameter, $g = 9.8$ m s^{-2} is gravitational acceleration, ρ_l is solution density, $\rho_a = 1.23$ kg m^{-3} is air density, and σ_l is solution surface tension. The estimated bubble diameter varied between 1.9 and 2.1 mm for the salt solutions studied here, as summarized in Table 1.

Typically bubble rise is driven by the buoyancy of the less-dense air relative to the more-dense salt solution. The velocity of the rising bubble may vary by ±50% depending on the concentration of surfactants in solution (Clift et al. 1978, p. 172), resulting in an estimated range for the bubble velocity of 10 to 30 cm s^{-1} for the 2-mm bubble diameters produced by our apparatus. The corresponding range for Reynolds numbers ($Re = \rho_l\, d_b\, v_b/\mu_l$) is 200 to 600.

At the surface, the upward motion slows on approaching the point of neutral buoyancy. Surface forces control the film covering the bubble, limiting the rate at which liquid drains from the film into the liquid reservoir. Vrij and Overbeek (1968) estimated the film thickness at the point of rupture from a balance on the forces between the air inside the rising bubble and the air at the liquid surface:

$$t = 0.267((A^2(d_b/2)^2)/(6\sigma_l P))^{1/7} \quad [2]$$

where A is the Hamaker constant for water and has the value 3.7×10^{-20} J (Israelachvili 1992), P is the capillary pressure of the draining film, and the values 6 and 7 are experimentally determined constants for the bubble bursting system (Chaudhari and Hofmann 1994). In these experiments, the estimated film thickness varied between 55 and 60 nm, as summarized in Table 1.

When the film bursts, a range of submicron particles including those smaller than 20 nm diameter are produced. If Equation (2) were sufficient to capture the factors controlling particle formation, then we would expect particle size to vary with the predicted film thickness at rupture. Composition controls density, viscosity, and intermolecular interactions in solution that affect film drainage and thinning. The rupture thickness controls particle properties and is controlled by the composition of the solution, making particle size a consequence of solution composition.

This work uses two approaches to analyze the impact of chemical composition on the film thinning process that controls particle formation from bubble bursting. The first approach is suggested by work in which Lessard and Zieminski (1971) identified threshold concentrations to describe the observed transition in the effect of ions on solution properties. This transition provides an empirical basis for normalizing concentrations

TABLE 1
Solution properties for NaCl, NaBr, and NaI solutions

Salt	NaCl		NaBr		NaI	
Solution concentration [mol kg^{-1}]	0.0014	1.7	0.0014	3.4	0.0014	1.7
Density[a,b] [kg m^{-3}]	1000	1064	1000	1237	1000	1193
Surface Tension[b,c,d] [mN m^{-1}]	72.0	74.5	72.0	76.1	72.0	74.0
Viscosity[b] [mPa s]	1.00	1.17	1.00	1.41	1.00	0.943
Bubble Diameter [mm] (Eqn. 1)	2.07	2.05	2.07	1.96	2.07	1.97
Capillary Pressure[e] [Pa] ($4\sigma/d_b$)	139	146	139	155	139	151
Film Thickness [nm] (Eqn. 2)	58.7	57.9	58.7	56.5	58.7	57.1
Solubility[a,b] [mol kg^{-1}]	6.15		11.3		12.3	
Electronegativity[a] [J kg^{-1}]	1.37×10^7		0.713×10^7		0.436×10^7	
Transition Concentration[f,g] [mol kg^{-1}]	0.18		0.22		0.12	
Eo at Transition[g] (Eqn. 3)	0.581		0.583		0.582	
Eo (Eqn. 3)	0.581	0.586	0.581	0.612	0.581	0.610
Normalized Solution Concentration[g]	0.008	9.9	0.007	19	0.015	17
Mean Diameter[g] [nm]	25	73	23	100	24	130
Number Concentration[g] [cm^{-3}]	2.4×10^5	8.0×10^5	3.4×10^5	2.2×10^6	3.5×10^5	1.4×10^6
Mass Concentration[g] [μg m^{-3}]	1.8×10^{-11}	2.6×10^{-7}	1.5×10^{-11}	9.7×10^{-7}	1.7×10^{-11}	4.8×10^{-7}

[a]Lide 2003; [b]Washburn et al. 1928; [c]Weissenborn and Pugh 1996; [d]Abramzon and Gaukhberg 1993; [e]Israelachvili 1992; [f]Lessard and Zieminski 1971; [g]This work (NaI).

of three different Na salts. The second type of analysis incorporates both buoyant and surface forces in the dimensionless Eotvos number. The advantage of this approach is its generality to multicomponent and organic mixtures for which threshold concentrations have not been tabulated.

Similarities in salt solution properties are evident when the concentration for each salt is normalized to a threshold concentration, as suggested by Lessard and Zieminski (1971). Their work has suggested that since ions both retard and enhance the diffusion of water molecules, this threshold represents a transition between these two competing effects, which is illustrated by the sharp cutoff of bubble coalescence behavior for sufficiently concentrated salt solutions (see Figure 4 of Lessard and Zieminski 1971). Decreased coalescence of gas bubbles as well as decreased rates of increase of solution entropy and water self-diffusion also become evident at similar threshold concentrations. Inhibition of bubble coalescence produces foaminess and the associated small bubbles which burst at the ocean surface. For this reason, the first approach supposes that the number, size, and mass of particles produced will be controlled by solution concentration after normalizing to the characteristic threshold concentration for the salt. This approach proposes that the same transition that controls ionic entropy and self-diffusion in aqueous solutions also governs the bubble bursting process.

The Eotvos number, also called the Bond number, is used as the second approach to identifying a characteristic solution property, quantifying the ratio of buoyant to surface forces for the bubble:

$$Eo = g(\rho_1 - \rho_a)d_b^2/\sigma_1 \qquad [3]$$

(Clift et al. 1978, p. 26). High values for liquid density and bubble diameter increase *Eo*, while increasing bubble density and liquid surface tension can slow this increase.

MEASUREMENTS

Particle production from a bubbler based on the Blanchard and Syzdek (1988) design was measured for three Na salts: NaCl, NaBr, and NaI. The measurements detected particle number and Na mass in size-resolved particles by sequential size separation in a differential mobility analyzer and detection by a condensation particle counter and a flame photometer, as shown in Figure 1. The size-dependent response of the detector has been calibrated by comparison to atomized NaCl particles, providing an effective measurement range of 150 to 300 nm diameter. The calibration data in Figure 2 illustrate the measured detector response and its variability, shown with error bars representing the standard deviation of the measured voltage by the flame photometer.

Na mass distribution of ambient sea salt, atomized NaCl, and bubbled NaCl particles are shown in Figure 3. The ambient particles are much less concentrated than the atomized and bubbled NaCl laboratory standards. Since the absolute value of the concentrations shown depend on different rates of bubbling and dilution, the common features are the size and shape of the Na particle distributions smaller than 300 nm. In addition, the peak in the particle size distribution at 70 nm in clean marine air provides evidence for a small sea salt mode similar to that observed in laboratory bubbling experiments. All three sources of generated sea salt particles show variability, with error bars representing one standard deviation of the measured values.

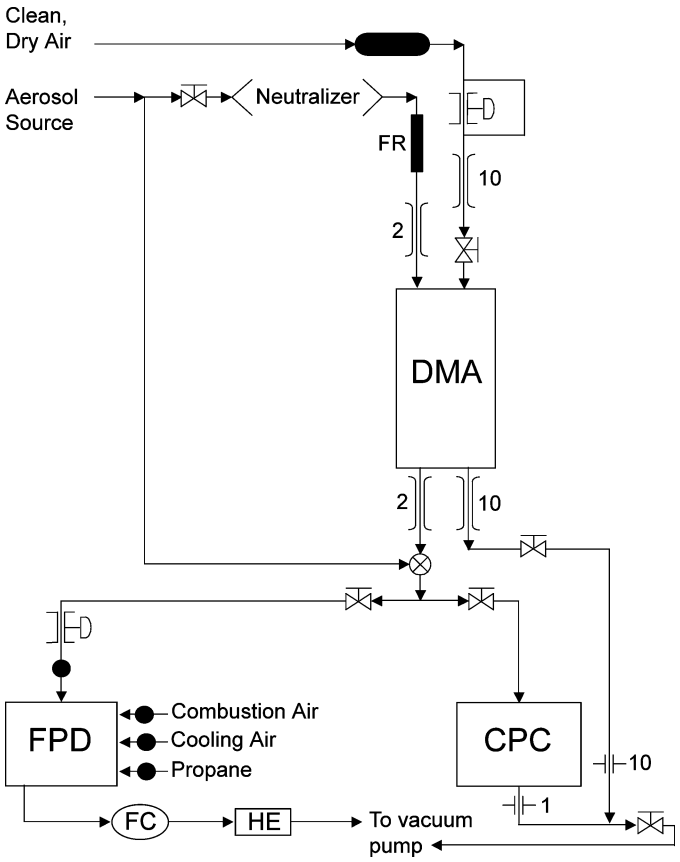

FIG. 1. Schematic of the salt particle counter (FC = flame check, HE = heat exchanger, FR = flow restrictor, DMA = differential mobility analyzer, CPC = condensation particle counter, FPD = flame photometric detector). Numbers indicate monitored flow rates in L min^{-1}.

RESULTS

To study the production of particles by bubble bursting, the concentration of ions in solution was varied over the maximum range possible for the bubbler and detector, being limited on the high side by bubbling consistency and on the low side by detection limits. These concentrations illustrate the relative increases and decreases in particle concentration with Na salt aqueous concentrations for the approximately constant bubbling conditions used here. The resulting concentrations range from 0.0014 to 1.71 mol kg^{-1}, and the changes in physical properties for these solutions are summarized in Table 1. The measured particle number and Na mass size distributions in

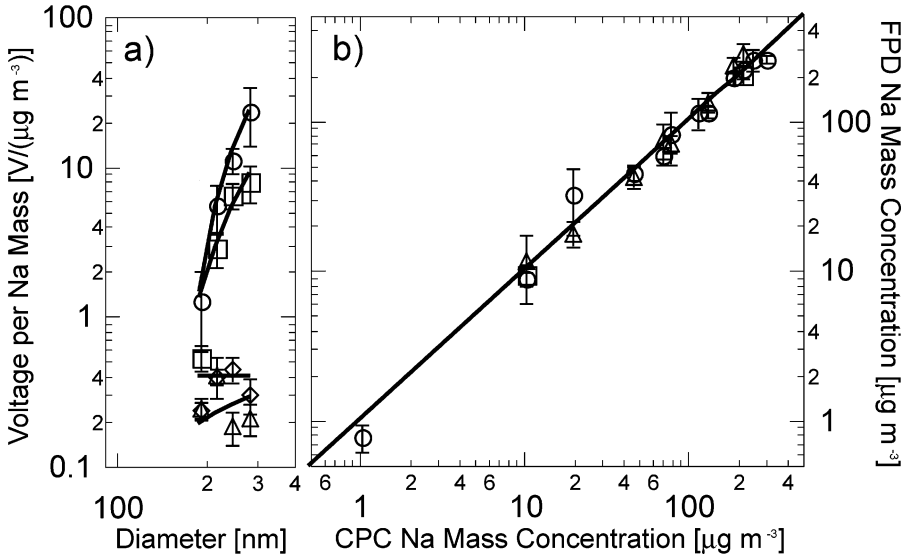

FIG. 2. Calibration of salt particle counter and comparison to condensation particle counter for Na particles: (a) Flame photometer voltage response to Na mass ratio for 2 minute scans at 10.1 μg m^{-3} (circles), $R^2 = 0.99$; 19.8 μg m^{-3} (squares), $R^2 = 0.92$; 189 μg m^{-3} (diamonds), $R^2 = 0.90$; 215 μg m^{-3} (triangles), $R^2 = 0.63$. Vertical error bars indicate variability by the standard deviation of all measured values. (b) Comparison of derived mass of Na for flame photometer and condensation particle counter for scans of 2 min (triangles), 8 min (circles), and 20 min (squares).

Figure 4, show the increase of particle size and number with solution concentration. The modal mean diameter varied from 20 to 150 nm, with number concentrations between 3×10^5 and 2×10^6 cm^{-3}. The results from all three Na salts show that both particle size and number generally increase with concentration, with comparable increases in particle mass. The three Na salts show similar behavior in size, number, and shape of the particle distribution. The variability in the observed distributions increases at high concentrations, where bubble production was more sporadic. This variability in the size distributions produced is reflected in the error bars, each representing one standard deviation of the measured values.

Three particle properties were used to characterize particle production—modal mean diameter, modal number concentration, and modal mass concentration. The dependence of these properties on solution concentration and associated fluid properties (including calculated values for film thickness, Weber number, Capillary number, ionic strength, normalized solution concentration, Eotvos number) was investigated to identify the best fit parameterizations that can be generalized for all three salts,

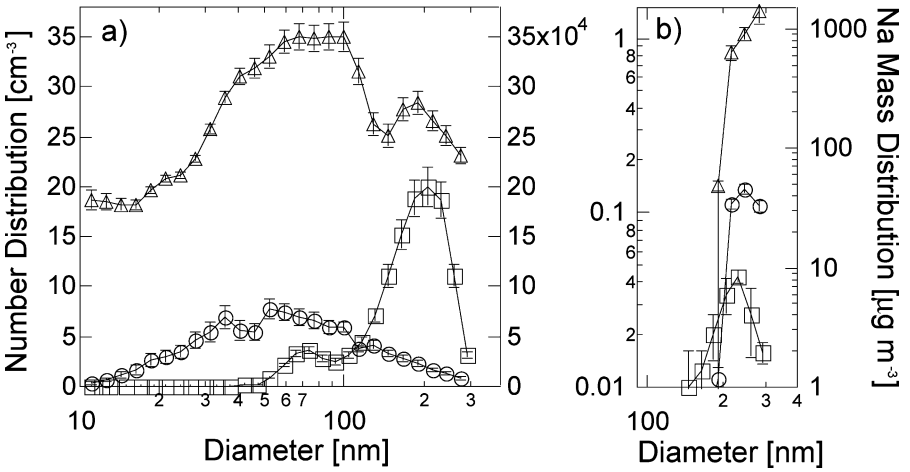

FIG. 3. Comparison between atomizer, bubbler, and field data: (a) number size distribution and (b) Na mass distribution. Symbols represent atomizer (triangles, inner right axis), bubbler (circles, far right axis), and PELTI field data (squares, left axis). Vertical error bars indicate variability by the standard deviation of all measured values.

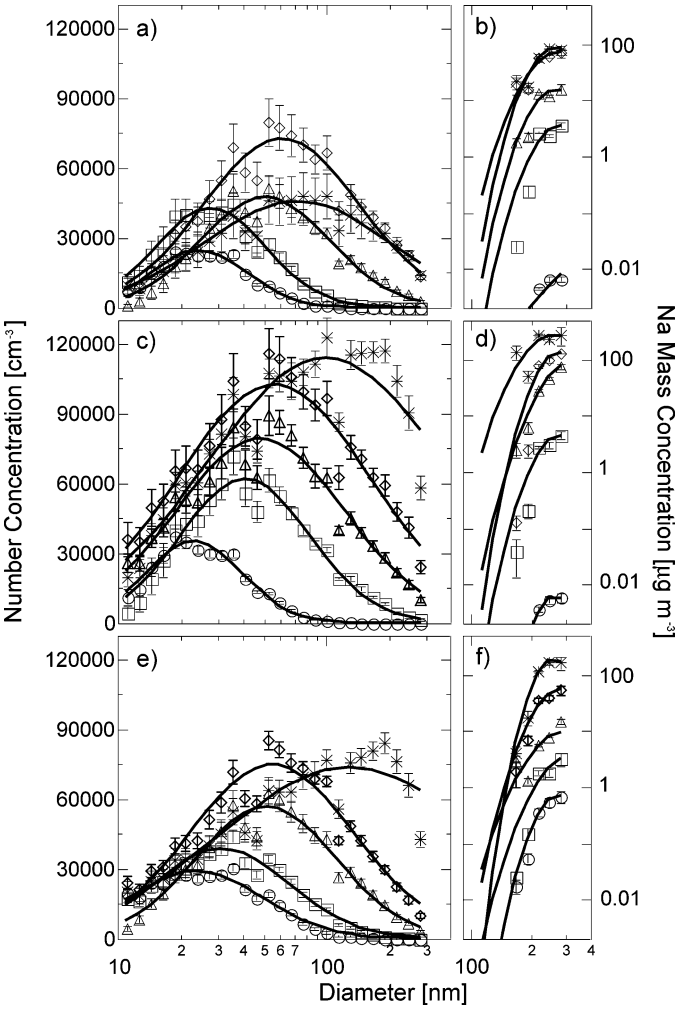

FIG. 4. Number size distributions and Na mass distributions for bubbling of Na salt solutions: (a) Number size distributions and (b) Na mass distributions for NaCl solutions with 0.18 μg m^{-3} (circles), 8.9 μg m^{-3} (squares), 45 μg m^{-3} (triangles), 223 μg m^{-3} (diamonds), 260 μg m^{-3} (asterisks), (c) size distributions, and (d) mass distributions for NaBr solutions with 0.015 μg m^{-3} (circles), 11 μg m^{-3} (squares), 160 μg m^{-3} (triangles), 362 μg m^{-3} (diamonds), 969 μg m^{-3} (asterisks), (e) Size distributions, and (f) mass distributions for NaI solutions with 1.6 μg m^{-3} (circles), 7.0 μg m^{-3} (squares), 33 μg m^{-3} (triangles), 139 μg m^{-3} (diamonds), 478 μg m^{-3} (asterisks). Vertical error bars indicate variability by the standard deviation of all measured values.

and potentially for more complex mixtures. The predicted film thickness decreases with the normalized solution concentration while the observed mean diameter increases for all three Na salts. The dependence on Weber and Capillary numbers varied greatly for the three salts, failing to produce a prediction that represented all three salts. The ionic strength of the solution increases with the solution concentration, revealing similar functional relationships. Particle diameter, number concentration, and mass concentration increase with solution concentration at slightly different rates for each Na salt. The two sets of relationships that collapsed the measured particle properties for all three salts were the normalized solution concentration ob-

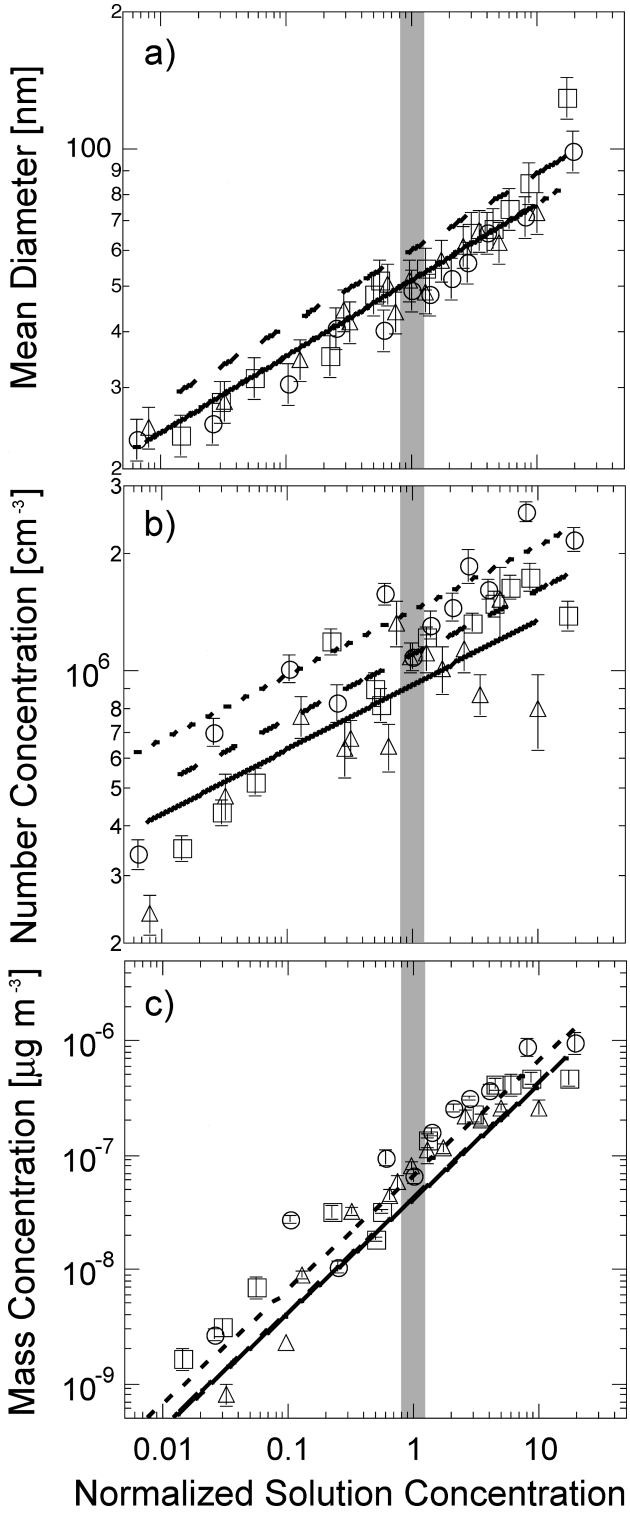

FIG. 5. Properties of particles produced by bubble bursting as functions of normalized solution concentration: (a) Mean diameter, (b) Modal number concentration of particles, (c) Modal mass concentration of particles. For all panels, symbols are measured values and lines are parameterizations for NaCl (triangles, solid line), NaBr (circles, short-dashed line), and NaI (squares, long-dashed line). The shaded region indicates the threshold concentration at $C = 1$. Vertical error bars represent twice the detection limit for each measurement.

tained with the threshold concentration approach and the Eotvos number.

Threshold Concentration Approach

The normalized solution concentration C is the ratio of the measured solution concentration to the transition concentrations reported for each salt (Lessard and Zieminski 1971): 0.18 mol kg^{-1} for NaCl, 0.22 mol kg^{-1} for NaBr, and 0.12 mol kg^{-1} for NaI. Figure 5 shows that particle diameter, number concentration, and mass concentration each increase similarly with normalized solution concentration. The uncertainty in the measured mean diameter is estimated to be $\pm 10\%$, based on the uncertainty in the modal fit and differential mobility analyzer flow rates. The uncertainties for number and mass concentration are shown as twice the detection limit, as these limits generally exceed other errors. The normalized solution concentrations succeeds in providing an abscissa that collapses particle characteristics for all three salts to the same parameterization for each particle property, as summarized in Table 2.

Particle mean diameter was parameterized to normalized solution concentration to the sixth root. This power law fit all three salts well ($R^2 = 0.94 - 0.98$) with similar prefactors (51–59). The modal number concentration was also best fit with a one-sixth power law, although the correlations were weak ($R^2 = 0.68 - 0.92$). The mass concentration of particles varied linearly with the normalized solution concentration, with high correlations ($R^2 = 0.85 - 0.91$). There is some variability in the slopes identified, although NaCl and NaI parameterizations are overlapping. The strong linear dependence of particle mass on normalized solution concentration indicates that this parameterization works well for the range of concentrations studied here, namely from 0.0014 to 3.4 mol kg^{-1}.

Eotvos Number Approach

The second approach to understanding particle production uses the ratio of buoyant to viscous forces of the aqueous solution to predict the number, size, and mass of particles produced. Figure 6 shows the changes in mean particle size, number, and Na mass with Eo. The similarity of the resulting parameterizations of particle properties to the Eotvos number for all three Na salts provides a strong indication that, for similar density solutions above the threshold concentration, particle production is dominated by surface forces. Below the threshold concentration, which corresponds to $Eo = 0.582 \pm 0.001$, there is a very strong dependence of particle properties on Eo, with a slope too steep to quantify given the measurement uncertainty. Above this value, linear parameterizations were obtained for modal mean diameter, number concentration, and mass concentration with Eo for all three salts. These parameterizations are given in Table 2.

The range of Eo is only slightly above that of pure water (0.581) for the entire range of concentrations studied, since density and surface tension vary only slightly for aqueous Na solutions. Within this limited range, two distinct regimes of particle formation are evident. For low solution concentration, there are very rapid increases in the particle size, number, and mass, independent of Eo.

At higher solution concentrations, the buoyant force increases relative to the surface force above the transition value at $Eo = 0.582 \pm 0.001$. In this large Eo regime, mean diameter and particle number concentration continue to increase, although

TABLE 2
Parameterizations of measured particle properties to normalized solution concentration and Eotvos number

	Normalized solution concentration		Eotvos number	
NaCl	$0.008 < C < 9.8$		$0.581 < Eo < 0.590$	
NaBr	$0.007 < C < 19$		$0.583 < Eo < 0.612$	
NaI	$0.014 < C < 17$		$0.582 < Eo < 0.638$	
Mean Diameter [nm]				
NaCl	$(51)C^{1/6}$	$R^2 = 0.98$	$(10^3)(-2.8 + 4.4Eo)$	$R^2 = 0.88$
NaBr	$(51)C^{1/6}$	$R^2 = 0.97$	$(10^3)(-1.0 + 1.8Eo)$	$R^2 = 0.98$
NaI	$(59)C^{1/6}$	$R^2 = 0.94$	$(10^3)(-1.5 + 2.6Eo)$	$R^2 = 0.99$
Number Concentration [cm^{-3}]				
NaCl	$(9.1 \times 10^5)C^{1/6}$	$R^2 = 0.68$	$(10^7)(-3.7 + 6.5Eo)$	$R^2 = 0.27$
NaBr	$(1.4 \times 10^6)C^{1/6}$	$R^2 = 0.92$	$(10^7)(-2.2 + 4.1Eo)$	$R^2 = 0.76$
NaI	$(1.1 \times 10^6)C^{1/6}$	$R^2 = 0.91$	$(10^7)(-0.95 + 1.8Eo)$	$R^2 = 0.55$
Mass Concentration [$\mu g\ m^{-3}$]				
NaCl	$(3.8 \times 10^{-8})C$	$R^2 = 0.85$	$(\ 10^{-5})(-2.7 + 4.6Eo)$	$R^2 = 0.85$
NaBr	$(6.2 \times 10^{-8})C$	$R^2 = 0.91$	$(\ 10^{-5})(-1.8 + 3.1Eo)$	$R^2 = 0.94$
NaI	$(3.9 \times 10^{-8})C$	$R^2 = 0.85$	$(10^{-5})(-0.59 + 1.1Eo)$	$R^2 = 0.75$

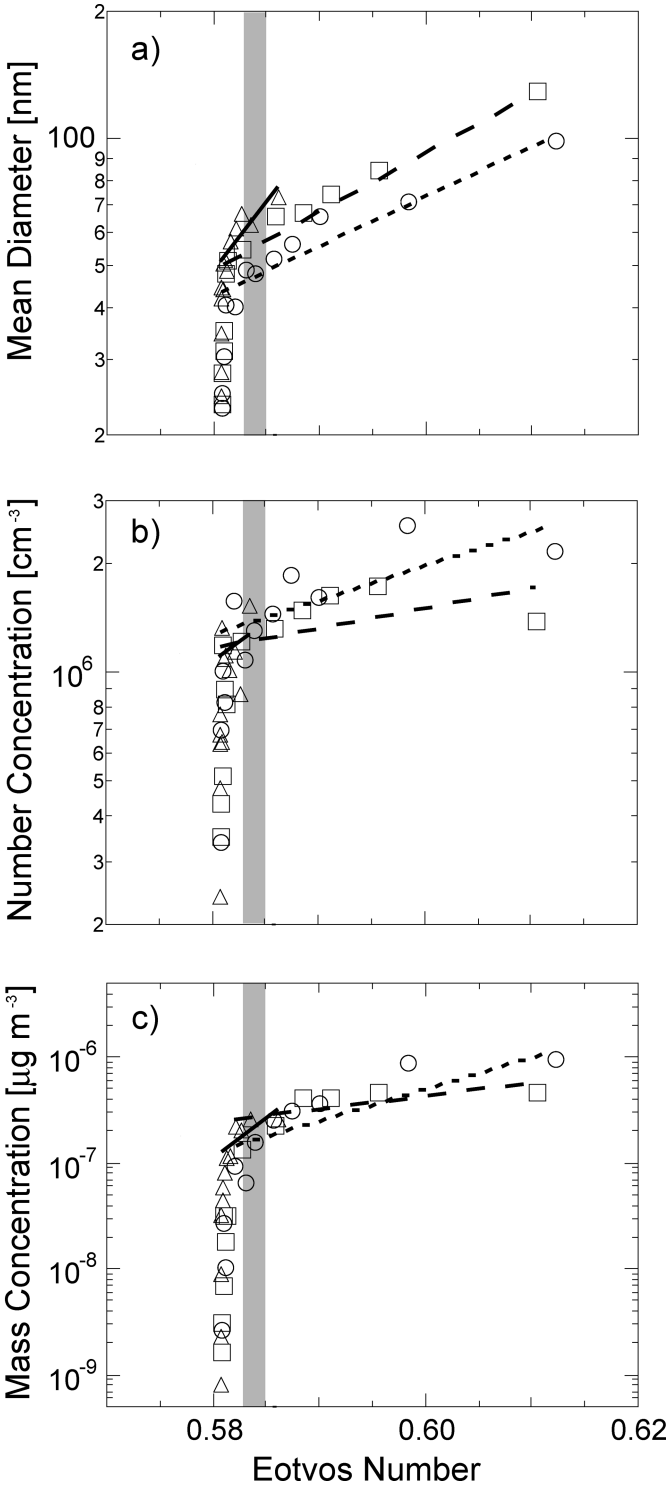

FIG. 6. Properties of particles produced by bubble bursting as functions of Eotvos number (a) Modal mean diameter, (b) Modal number concentration of particles, (c) Modal mass concentration of particles. For all panels, symbols are measured values and lines are parameterizations for NaCl (triangles, solid line), NaBr (circles, short-dashed line), and NaI (squares, long-dashed line). The shaded region indicates $Eo = 0.582 \pm 0.001$, the value of the Eotvos number at the threshold concentration. Vertical error bars are the same as in Figure 5 and are omitted for clarity of presentation.

the rate of increase is reduced relative to lower *Eo*. The particle diameter increases from 1.2 ± 0.1 to 3.1 ± 0.5 and matches a linear parameterization well in this range ($R^2 = 0.88 - 0.99$). The modal particle number concentration increases from $(1.1 \pm 0.1) \times 10^6$ to $(2.5 \pm 0.5) \times 10^6$ cm^{-3}, much slower than the slope below $Eo = 0.582 \pm 0.001$. The parameterizations of number concentrations show weak correlations to measured values ($R^2 = 0.27$–0.76). The mass concentration shown in Figure 6 behaves similarly to the other particle properties. Above $Eo = 0.582 \pm 0.001$, as the buoyant force relative to the surface force increases, the normalized Na mass rapidly decreases and then slowly stabilizes. The particle mass concentration decreases from $(8.0 \pm 0.5) \times 10^{-9}$ to $(2.0 \pm 0.5) \times 10^{-9}$. The correlation to linear parameterizations above the transition is good for NaBr and weaker for NaCl and NaI ($R^2 = 0.75$–0.94). The poorer quality of the NaCl fit is largely due to the small range of *Eo* that was measured above $Eo = 0.582 \pm 0.001$.

DISCUSSION

A complete mechanistic interpretation of particle production is not yet possible by experimental or theoretical approaches because we cannot capture both the macroscopic fluid mechanics of film rupture and the microscopic intermolecular interactions of strong ionic solutions. However, the parameterizations to normalized solution concentration and *Eo* identified in this work are sufficient to predict the essential characteristics of particle production.

The effectiveness of the threshold concentration for normalizing solution concentrations suggests that the thresholds found in ion-induced properties of NaCl, NaBr, and NaI solutions also distinguish their particle formation processes. The similarity in the observed behaviors of different Na salts is consistent with the expected role of viscosity and microscopic ionic interactions in delaying the drainage of the bubble film before it ruptures (Garrett 1967; Craig et al. 1993). The dependence of both number concentration and mean diameter on the one-sixth power of the aqueous Na solution concentration provides an important starting point for speculating that ionic forces may retard fluid motion to limit the bubble bursting process, although more evidence is needed to identify the controlling mechanism.

The consistency of the relationships of particle properties to *Eo* for different salts indicates that the forces controlling the bubble bursting mechanism are described effectively by the ratio of buoyant and surfaces forces. The change in dependence of particle properties with *Eo* at the threshold concentration indicates a further link to the observed effect of ions on diffusion in solutions (Lessard and Zieminski 1971). The regime of $Eo > 0.582 \pm 0.001$ shows a linear dependence of particle size, mass, and number concentration on *Eo*. As *Eo* approaches the value for pure water, namely $Eo < 0.582 \pm 0.001$, the number and size of particles formed decrease greatly with negligible changes in *Eo*. The linear dependence provides evidence that the ratio of buoyant and surface forces controls particle production

at higher ionic concentrations. The dropoff at low concentrations provides the threshold value below which particle production is negligible and *Eo* is indistinguishable from that of pure water.

These two regimes in *Eo* number, in addition to the previous observations of threshold behavior in ionic solutions, reflect the complexities of interfacial processes for ionic solutions. The collapse of these results to common curves for three Na salts suggests that the relationships described here may have predictive ability for other aqueous solutions. More complex chemical compounds and mixtures should also be studied in order to build our understanding of particle production in complex environmental systems, such as the oceans and their surface microlayers.

REFERENCES

Abramzon, A. A. and Gaukhberg, R. D. (1993). Surface Tension of Salt Solutions. *Russian J. Appl. Chem.* 66:1473–1480.

Aluwihare, L. I., Repeta, D. J., and Chen, R. F. (1997). A Major Biopolymeric Component to Dissolved Organic Carbon in Surface Sea Water. *Nature* 387:166–169.

Blanchard, D. C. and Syzdek, L. D. (1977). Production of Air Bubbles of a Specified Size. *Chem. Engineer. Sci.* 32:1109–1112.

Blanchard, D. C. and Syzdek, L. D. (1988). Film Drop Production as a Function of Bubble Size. *J. Geophys. Res.* 93:3649–3654.

Blanchard, D. C. and Woodcock, A. H. (1957). Bubble Formation and Modification in the Sea and its Meteorological Significance. *Tellus* 9:145–158.

Chaudhari, R. and Hofmann, H. (1994). Coalescence of Gas Bubbles in Liquids. *Rev. Chem. Engineer.* 10:131–190.

Clarke, A., Kapustin, V., Howell, S., Moore, K., Lienert, B., Masonis, S., Anderson, T., and Covert, D. (2003). Sea-Salt Size Distributions from Breaking Waves: Implications for Marine Aerosol Production and Optical Extinction Measurements during SEAS. *J. Atmos. Ocean. Technol.* 20:1362–1374.

Clift, R., Grace, J. R., and Weber, M. E. (1978). *Bubbles, Drops, and Particles.* Academic Press, New York.

Cloke, J., McKay, W. A., and Liss, P. S. (1991). Laboratory Investigations into the Effect of Marine Organic Material on the Sea-Salt Aerosol Generated by Bubble Bursting. *Marine Chem.* 34:77–95.

Craig, V. S. J., Ninham, B. W., and Pashley, R. M. (1993). Effect of Electrolytes on Bubble Coalescence. *Nature* 364:317–319.

Garrett, W. D. (1967). Stabilization of Air Bubbles at the Air-Sea Interface by Surface-Active Material. *Deep Sea Res.* 14:661–672.

Guichard, J. C. and Lamauve, M. (1988). The Laboratory Production of the Bubbling Fraction of the Marine Aerosol-Application to Polluted Seawater. *Atmos. Environ.* 22:1835–1838.

Israelachvili, J. N. (1992). *Intermolecular and Surface Forces, Second Edition.* Academic Press, New York.

Lessard, R. R. and Zieminski, S. A. (1971). Bubble Coalescence and Gas Transfer in Aqueous Electrolytic Solutions. *Indus. Engineer. Chem. Fund.* 10:260–269.

Lide, D. R., Ed. (2003). *CRC Handbook of Chemistry and Physics.* CRC Press, New York.

Martensson, E. M., Nilsson, E. D., de Leeuw, G., Cohen, L. H., and Hansson, H.-C. (2003). Laboratory Simulations and Parameterization of the Primary Marine Aerosol Production. *J. Geophys. Res.* 108:DOI10.1029/2002JD002263.

O'Dowd, C. D., Smith, M. H., Consterdine, I. E., and Lowe, J. A. (1997). Marine Aerosol, Sea-Salt, and the Marine Sulphur Cycle: A Short Review. *Atmos. Environ.* 31:73–80.

Russell, L. M., Pandis, S. N., and Seinfeld, J. H. (1994). Aerosol Production and Growth in the Marine Boundary Layer, *J. Geophys. Res.* 99:20989–21003.

Smith, M. H., Park, P. M., and Consterdine, I. E. (1993). Marine Aerosol Concentrations and Estimated Fluxes over the Sea. *Q. J. Royal Meteorol. Soc.* 119:809–824.

Spiel, D. E. (1997). A Hypothesis Concerning the Peak in Film Drop Production as a Function of Bubble Size. *J. Geophys. Res.* 102:1153–1161.

Spiel, D. E. (1998). On the Births of Film Drops from Bubbles Bursting on Seawater Surfaces. *J. Geophys. Res.* 103:24907–24918.

Vrij, A. and Overbeek, J. T. G. (1968). Rupture of Thin Liquid Films Due to Spontaneous Fluctuations in Thickness. *J. Amer. Chem. Soc.* 90:3074–3078.

Washburn, E. W., West, C. J., and Dorsey, N. E., Eds. (1928). *International critical tables of numerical data, physics, chemistry, and technology.* McGraw-Hill, New York.

Weissenborn, P. K. and Pugh, R. J. (1996). Surface Tension of Aqueous Solutions of Electrolytes: Relationship with Ion Hydration, Oxygen Solubility, and Bubble Coalescence. *J. Col. Interface Sci.* 184:550–563.